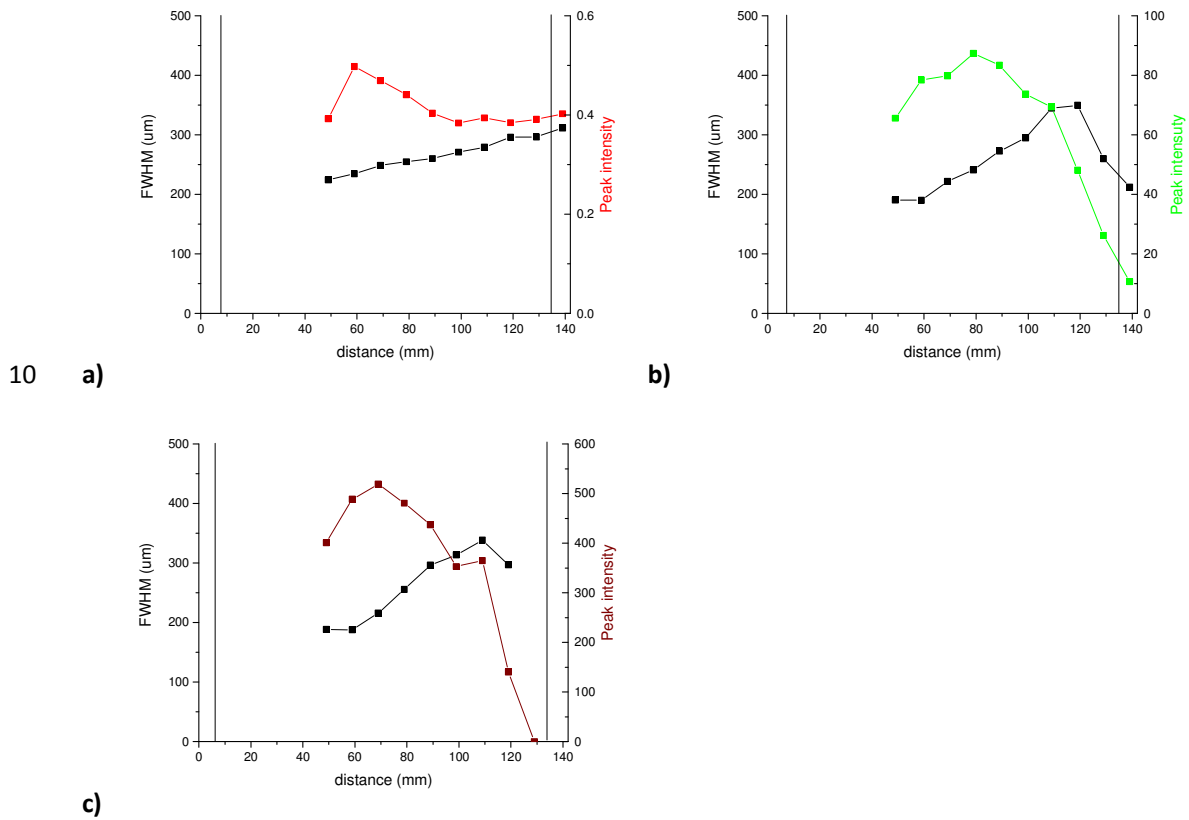


**5 S1 Beam size and intensity distribution**

Beam sizes were measured using a CCD (Thorlabs DCC1545M-GL). The measured light intensity was calibrated using a power sensor (Thorlabs S121C). Images were analysed using ImageJ software (Figure S1). The peak intensities of 1.9 W/mm<sup>2</sup> and 2.1 W/mm<sup>2</sup> have been obtained for the 532 and the 1064 nm channels, respectively.



**Figure S1. Diameters and non-calibrated intensities for probe beam a), 532 nm pump beam b) and 1064 nm pump beam inside the measurement chamber as a function of distance from the axicon.**

15 **S2 Heating curves**

Heating curves describe the average change of photodiode voltage during the modulation period (1/91 s for the 532 nm channel, 1/96 s for the 1064 nm channel). The curves were obtained by averaging the signal from several thousand intervals (Figure S2). Because in the infrared channel the signal is lower, the noise is more pronounced (Figure S2.b). The pump laser being switched ON during the first half of the interval induces exponential increase of the signal voltage. During the OFF phase an exponential reduction is observed. During the first half of the interval induces exponential increase of the signal voltage. During the OFF phase an exponential reduction is observed. The time constants for both channels are similar.

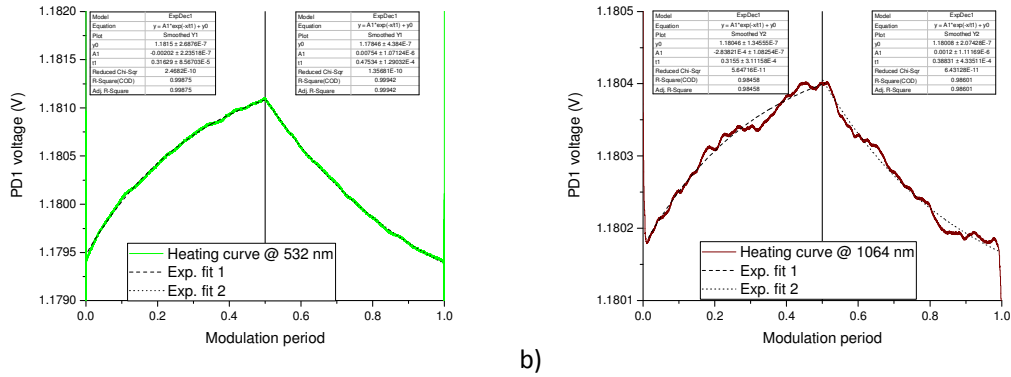


Figure S2. Average photodiode voltage during the heating and cooling parts of the modulation period for the 532 nm channel and the 1064 nm channel obtained for nigrosin particles. The durations of the modulation period are 11.1 ms and 10.4 ms for the corresponding channels. The curves are obtained by averaging the photodiode PD1 voltage over more than 10000 modulation periods.

### S3 Interferometer noise analysis

30 Interferometer noise was investigated by performing fast Fourier transform analysis of the  
interferometer signal on photodiode PD1 (Figure S3). Figure S4 shows signal, noise and noise/signal  
ratio for the selected modulation frequencies. In general, both signal and noise are larger at lower  
frequencies. There is also some increased noise at 60 and 240 Hz, the latter is most probably  
connected to the resonance of the beam splitter block. Measurement frequencies of 91 Hz and 96 Hz  
35 were selected for their best performance.

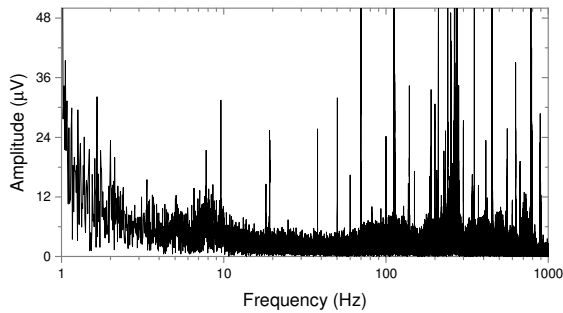
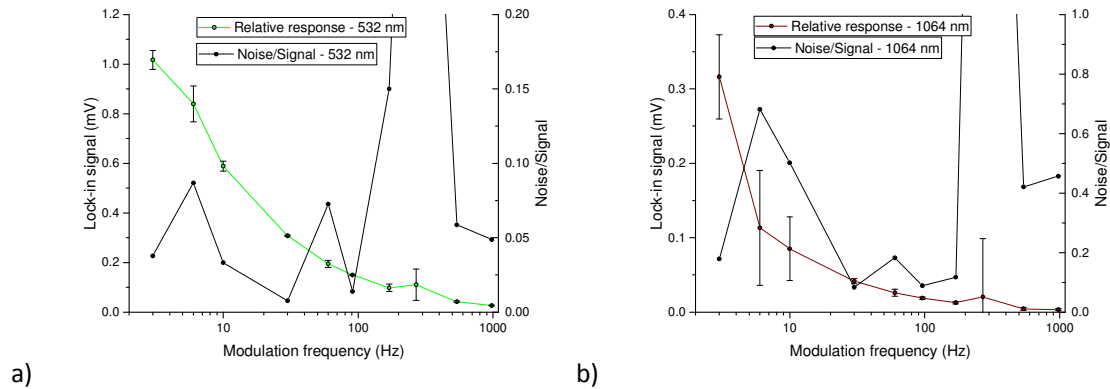
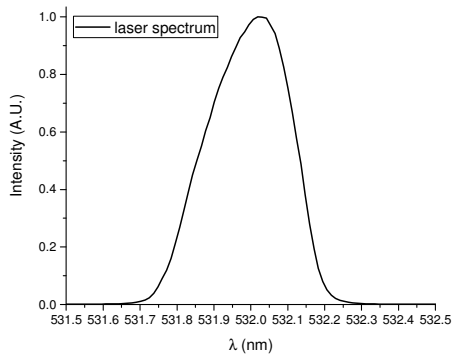


Figure S3. Fast Fourier transform of photodiode PD1 signal.

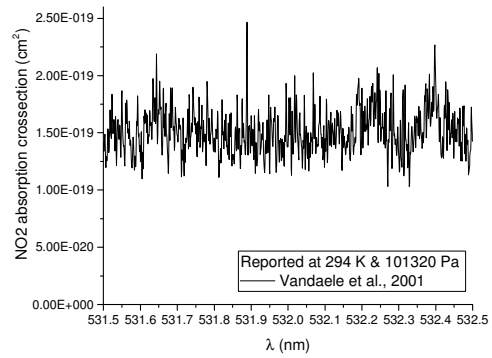


40 Figure S4. Lock-in signal and (noise/signal) ratio vs. modulation frequency for the 532 nm channel  
(a) and the 1064 nm channel (b). Noise was determined as the standard deviation of the signal. S4.  
NO<sub>2</sub> absorption

The 532 nm channel is calibrated using a mixture of 1 µmol/mol NO<sub>2</sub> in synthetic air. To calculate the  
absorption coefficient we need to know the absorption cross-section  $\sigma$  of NO<sub>2</sub> at the laser  
wavelength. We measured the emission spectrum of our 532 nm laser (Figure S5.a) and multiplied it  
45 with the absorption cross-section spectra (Figure S5.b) measured by Vandaele et al (2001). We  
obtained the absorption cross-section of  $1.47\text{E-}19\text{ cm}^2$ , which is close to  $1.45 \cdot 10^{-19}\text{ cm}^2$  obtained by  
Osthoff et al. (2006).



a)



b)

50 **Figure S5. Normalised spectrum of our 532 nm laser (a). High resolution absorption cross section of NO<sub>2</sub> (Vandaele et al., 2001)**

The absorption coefficient of 1 μmol/mol NO<sub>2</sub> is then:

$$b_{abs} = \frac{N}{V} \sigma, \tag{S1}$$

where N/V is a number density of NO<sub>2</sub> molecules:

$$\frac{N}{V} = 1 \text{ ppm} * \frac{N_{air}}{V} = 1 \text{ ppm} * \frac{p_0 * N_a}{R * T_0}. \tag{S2}$$

55 For 1 μmol/mol NO<sub>2</sub> at 100 kPa and 25 °C we obtain the absorption cross section of 357.3 Mm<sup>-1</sup>.

60

## S5 Determination of the optical properties of nigrosin

### S5.1 Measurements of the real part of the refractive index

65 A glass substrate with dimensions of 2 cm x 5 cm x 0.7 mm is placed in 1% solution of nigrosin in water. The solution slowly dried due to evaporation. After drying, a thin film of nigrosin dye remained on the surface. The nigrosin film was thick enough that almost no light was transmitted, so that the reflection from the glass substrate did not influence the measured reflection.

The refractive index of nigrosin was determined from measurements of the Brewster angle at two wavelengths, 632 nm and 1064nm. The laser output was polarized perpendicular to the substrate surface. Reflection of the laser light was measured as a function of the angle of incidence  $\theta$ .

70 At a certain angle all light that is polarized perpendicular to the substrate surface enters the sample. This angle is called the Brewster angle  $\theta_b$  for which:

$$\theta_b = \text{atan} \left( \frac{n_2}{n_1} \right). \quad (\text{S3})$$

In our case  $n_2$  is the refractive index of nigrosin and  $n_1$  is the refractive index of air, thus we can determine the refractive index of the dye by measurement of the Brewster angle.

75 Results for 633 nm:  $\theta_b = 61.12 \pm 0.36^\circ \rightarrow n = 1.81 \pm 0.01$

Results for 1064 nm:  $\theta_b = 61.59^\circ \pm 0.15^\circ \rightarrow n = 1.848 \pm 0.005$

Results at 633 nm agree with the literature value of 1.78 (Bluvshstein et al, 2017).

80

85

## S5.2 Absorbance of aqueous nigrosin solution

90 A spectrometer measures absorbance  $A$  of the sample with 10 mm optical path  $l$ . The absorption coefficient of the solution is calculated as:

$$b_{abs,sol} = \frac{atn}{l}, \quad (S4)$$

where the attenuation  $atn$  is:

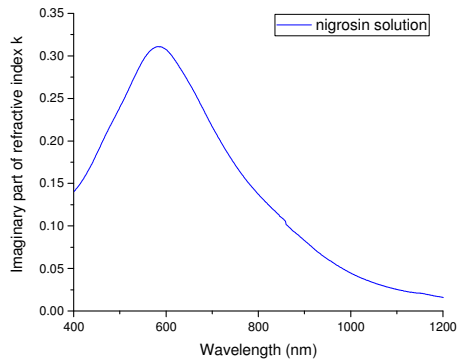
$$atn = A * \ln(10). \quad (S5)$$

95 The bulk absorption of the nigrosin is then:

$$b_{abs,bulk} = \frac{b_{abs,sol} * \rho_{nigrosin}}{\frac{m_{nigrosin}}{V_{sol}}}, \quad (S6)$$

where nigrosin density ( $\rho_{nigrosin}$ ) of  $1600 \text{ kg/m}^3$  and nigrosin mass concentration in the solution ( $m_{nigrosin}/V_{sol}$ ) of  $0.132 \text{ kg/m}^3$  is used. The imaginary part of the refractive index is then:

$$k = b_{abs,bulk} \frac{\lambda}{4\pi}. \quad (S7)$$



100

**Figure S6. Imaginary part of the refractive index of aqueous nigrosin solution determined by absorbance measurements.**

### S5.3 Absorbance measurement of solid nigrosin

105 Samples with different thicknesses (designated N2, N3, N4) in triplicate (designated a, b, c) were prepared (Figure S7). During drying of the nigrosin solution a thick edge was formed with uniform sample in the middle (Fig. S8). The absorbance of each sample was measured 3 times with the measurement beam in the middle of the sample (Fig. S8.a).

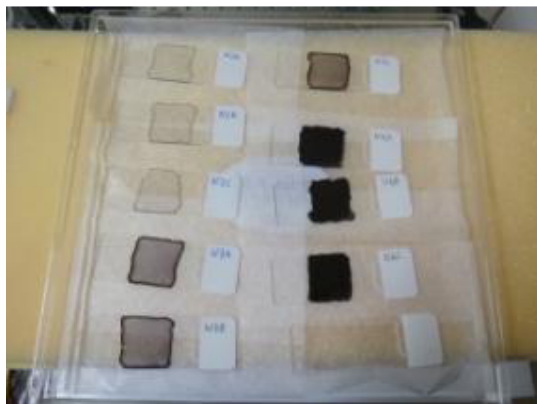


Figure S7. Solid nigrosin film samples on microscopy slides.

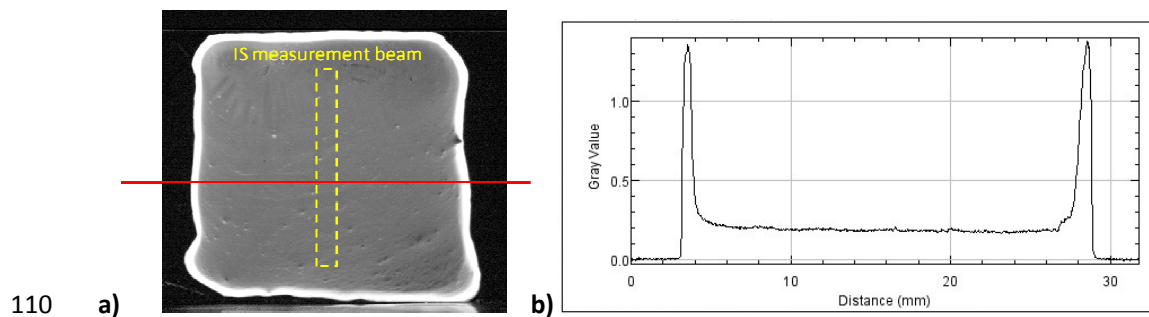
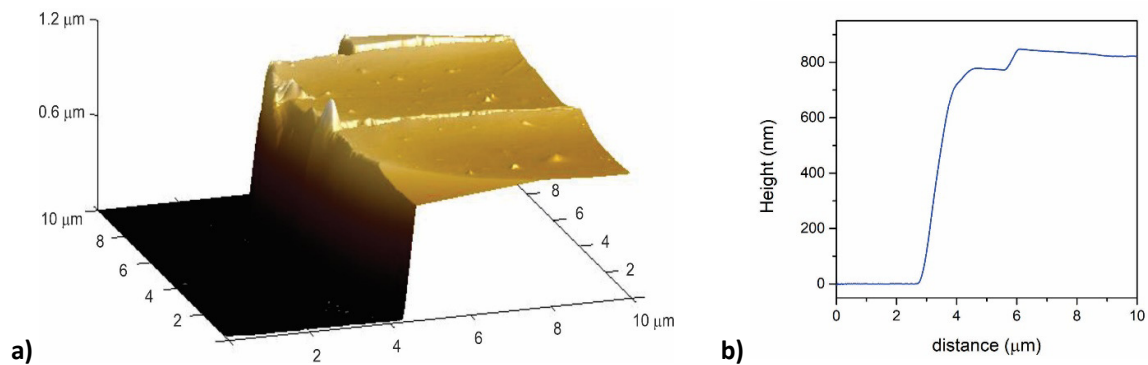


Figure S8. Absorbance image of nigrosin sample n3b (a) with marked position (dashed yellow line) of the measurement beam during integrating sphere measurements. Figure b shows a plot profile for the red line on the image a.

115 To calculate the imaginary part of the refractive index, the sample thickness was measured using atomic force microscopy. Sample thickness (Table S1) was determined by measuring the depth of the groove generated with a sharp plastic tip (Figure S9). Because the sample was destroyed during the sample preparation, only samples N2b, N3b and N4b were analysed.

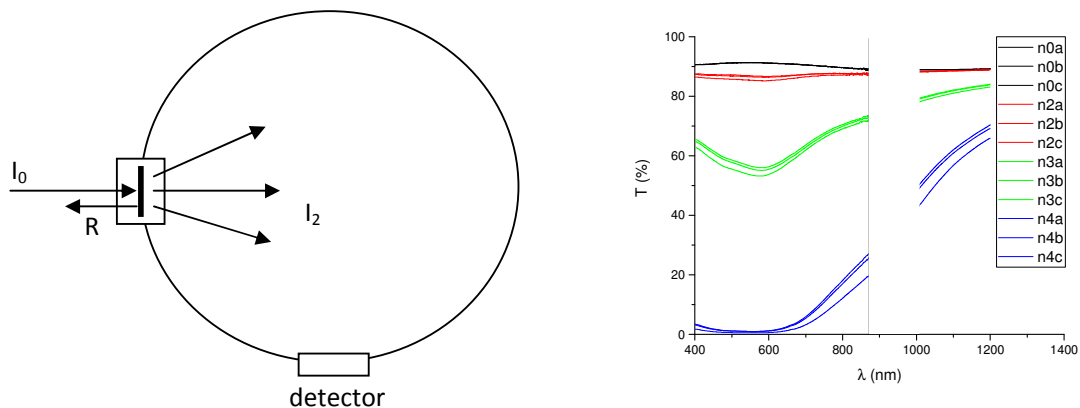


120 **Figure S9.3D image of the groove in the nigrosin sample measured by the atomic force microscope (a). Sample thickness is defined as a difference in plateau and depression height (b).**

**Table S1. Nigrosin sample thickness measured by atomic force microscope.**

Sample	Sample thickness
N2b	4-5 nm
N3b	65 nm
N4b	850 nm

125 The absorbance of solid nigrosin was measured in a Shimadzu UV-3600 UV-VIS-NIR Spectrophotometer. The sample was placed at the entrance to the integrating sphere with the nigrosin layer facing the measurement beam (Figure S10). Part of the light was reflected out of the integrating sphere.



130 a) b)

**Figure S10. Integrating sphere measurement setup (a). Measured transmittance  $T$  for different nigrosin samples (b).**

Absorbance measurements in the integrating sphere were validated with an absorptive neutral density filter (Thorlabs NE10B), which was measured both in the integrating sphere and with the collimated beam at 520 and 1064 nm (Figure S11). There is a good agreement between the measurements.

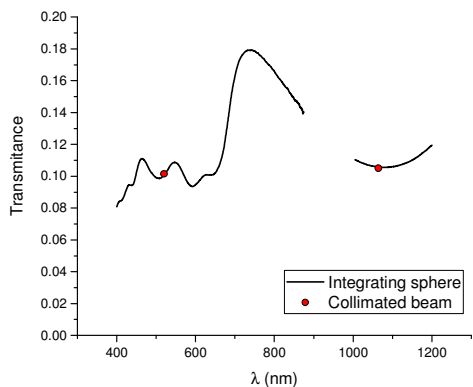
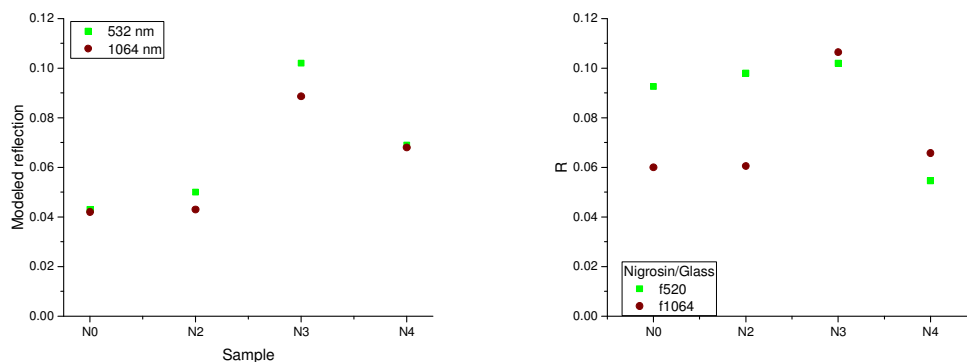


**Figure S11. Comparison between absorptive neutral density filter transmittance measured with integrating sphere and collimated beam at 520 and 1064 nm.**

140 The absorbance is calculated most reliably for the N4 and N0 sample pair, but it needs to be corrected for the illumination lost due to the reflection on the surface of the nigrosin layer. Fresnel equations were used to model the reflection of a thin absorptive film at 532 and 1064 nm (Figure S12.a). These values are compared to the measured reflectance (figure S12.b). Modeled reflectance is lower compared to measurements because it does not include reflection from the back of the glass substrate, which is most pronounced for samples N0 and N2 where the absorption of the returning beam is small. There seem to be some discrepancy between modelled and measured reflectance which can result in the uncertainty in refractive index of about 3%.

145



a)

b)

150 **Figure S12. a) Modelled reflectance of a clean glass substrate (N0) and nigrosin films N2b, N3b and N4b. The reflection from the back of the glass substrate is not taken into account. b) Reflectance measured using collimated beams on the samples N0b, N2b, N3b and N4b.**

Modelled reflectance was 4 % for clean sample (N0) and 7% for N4b sample at both wavelengths. The following correction scheme is used:

155 
$$A_c = A + \log \left( \frac{1-R_{N4b}}{1-R_{N0}} \right), \quad (S8)$$

the imaginary part of the refractive index was calculated similarly as for the aqueous solution. First the attenuation is calculated:

$$atn = A * \ln (10). \quad (S9)$$

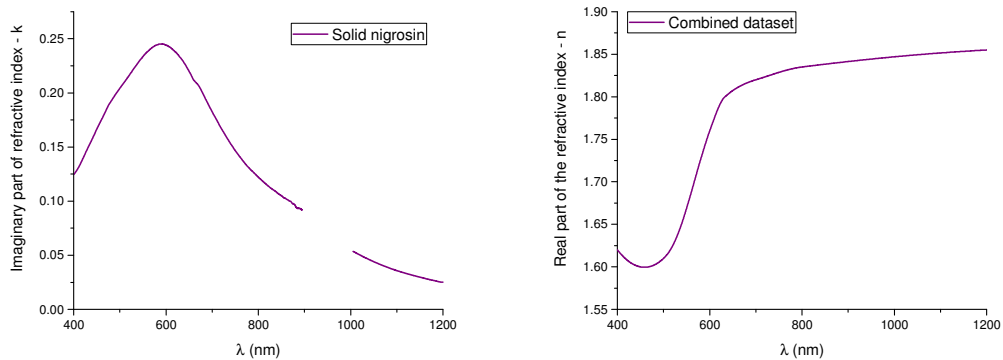
The bulk absorption coefficient can then be calculated for the sample of the thickness d:

160 
$$b_{abs,bulk} = \frac{atn}{d}. \quad (S10)$$

The imaginary part of the refractive index is then:

$$k = b_{abs,bulk} \frac{\lambda}{4\pi}. \quad (S11)$$

165 The imaginary part of the refractive index was determined in the 400-1200 nm range with some missing data between 900-1000 nm (Figure S13.a). The real part of the refractive index presented in Figure S13.b is a combination of Bluvshstein et al. (2017) data for the visible spectrum interpolated to the refractive index we have determined at 1064 nm. The proposed values are presented in Table S2.



170 **Figure S13. Proposed spectra of imaginary (a) and real (b) part of the refractive index of solid nigrosin.**

175 **Table S2. Refractive index of solid nigrosin. The real part of the refractive index is composed of measurements in the visible (Bluvshstein et al., 2017) and our measurement at 1064 nm. The imaginary part of the refractive index was determined by our absorbance measurements in the integrating sphere.**

$\lambda$ (nm)	n	k
400	1.620	0.125
420	1.608	0.140
440	1.602	0.158
460	1.600	0.175
480	1.602	0.192
500	1.610	0.204
520	1.625	0.216
540	1.652	0.228
560	1.688	0.238
580	1.726	0.244
600	1.760	0.244
620	1.789	0.238
640	1.803	0.227
660	1.811	0.212
680	1.816	0.199
700	1.820	0.183
720	1.823	0.167
740	1.827	0.153
760	1.830	0.141
780	1.833	0.131
800	1.835	0.122
820	1.836	0.115
840	1.838	0.108
860	1.839	0.102
880	1.840	0.096
900	1.841	0.090
920		
940		
960		
980		
1000	1.847	0.055
1020	1.848	0.050
1040	1.849	0.046
1060	1.850	0.042
1080	1.851	0.039
1100	1.852	0.036
1120	1.852	0.033
1140	1.853	0.031
1160	1.854	0.029
1180	1.854	0.027
1200	1.855	0.025

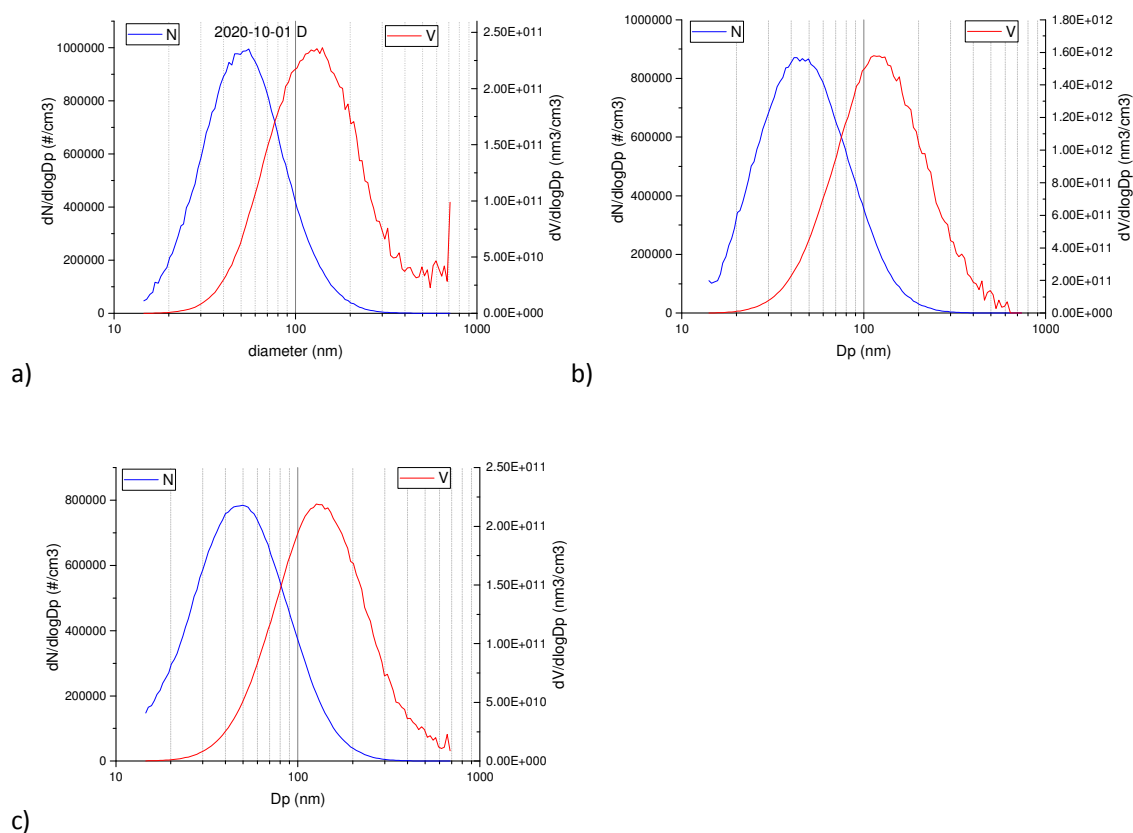
### S5.3 Mie calculation

180 Absorption coefficients for nigrosin are obtained using Mie calculation with the known refractive index and particle size distributions (Figure S14). The procedure was conducted during the AeroTox and Ljubljana 2021 campaigns. Size distributions below 400 nm were used for the calculation since the errors in the larger particle data results in an increased error. The following absorption ratios have been obtained for different experiments:

185 a) AeroTox 2020\_10\_01:  $b_{1064}/b_{532} = 0.0743$

b) Ljubljana 2020\_11\_22:  $b_{1064}/b_{532} = 0.0764$

c) Ljubljana 2021\_05\_07:  $b_{1064}/b_{532} = 0.0733$



190 **Figure S14. Particle size distributions determined during the following experiments: AeroTox 2020\_10\_01 (a), Ljubljana 2020\_11\_22 (b) and Ljubljana 2021\_05\_07 (c)**

## S6 Scanning electron microscopy of filter samples

195 Various aerosols were sampled on a Nuclepore® membrane. Diesel exhaust particles consist of small agglomerates with 2-4 globules and sizes between 80 and 180 nm (Figure S15). The agglomerates for the propane soot are much larger, 260-400 nm (Figure S16). Nigrosin samples show spherical particles with size increasing with the concentration of the nigrosin solutions used in the nebulizer (Figures 17, 18, 19).

200

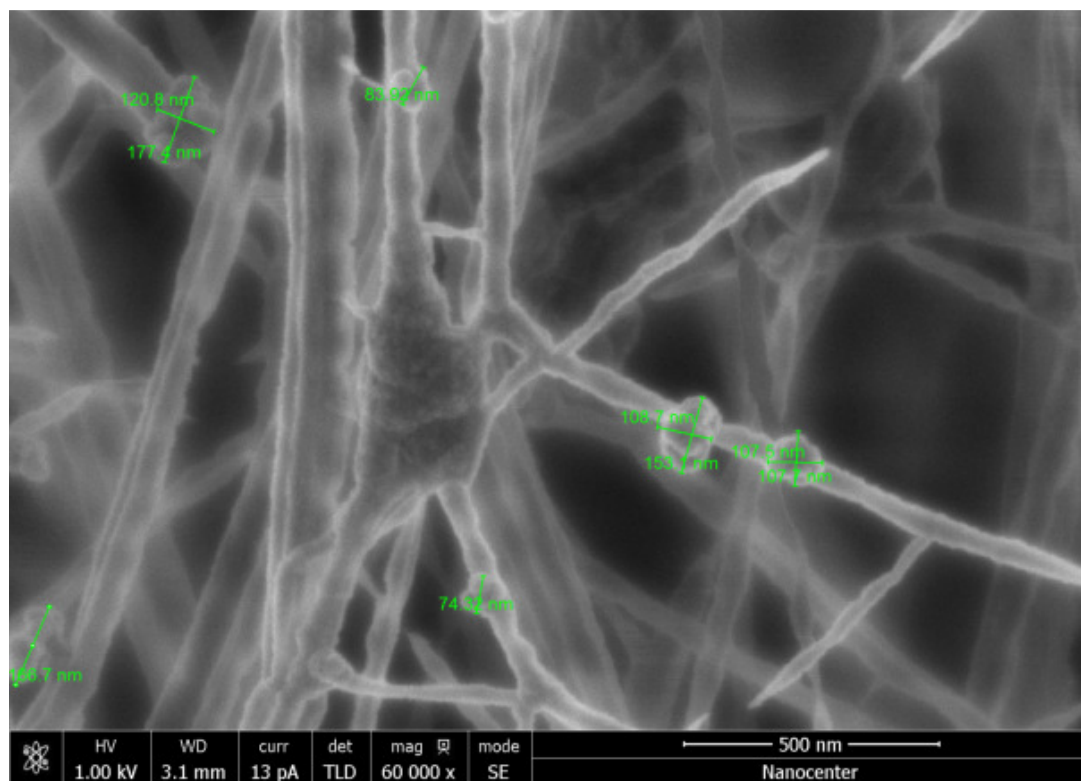


Figure S15. SEM image of particles from diesel exhaust (Image D3\_008)

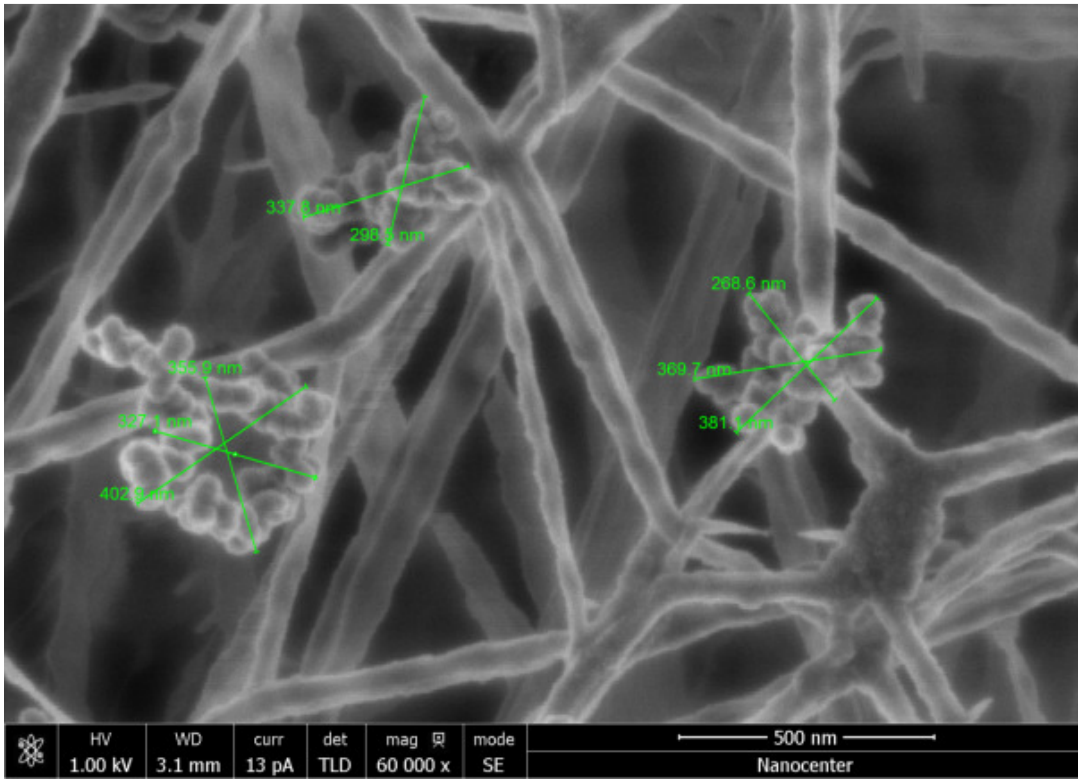


Figure S16. SEM image of propane soot particles (Image sp1\_005)

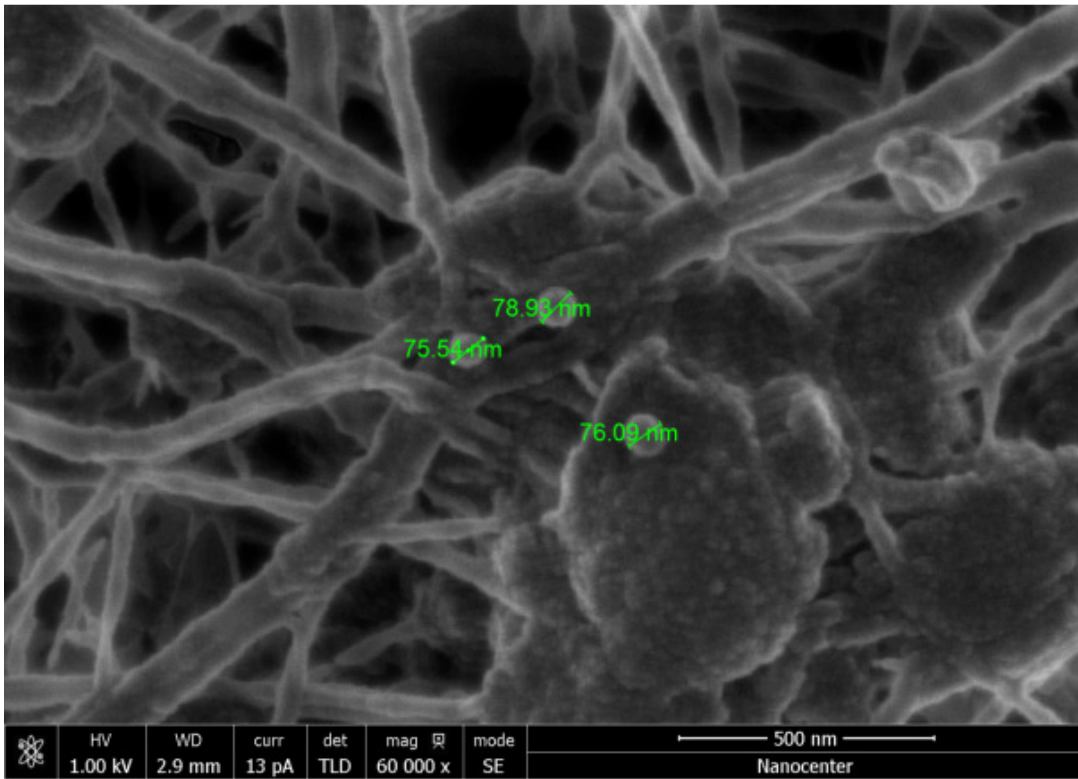


Figure S17. SEM image of N1 nigrosin particles (Image N1b\_004)

205

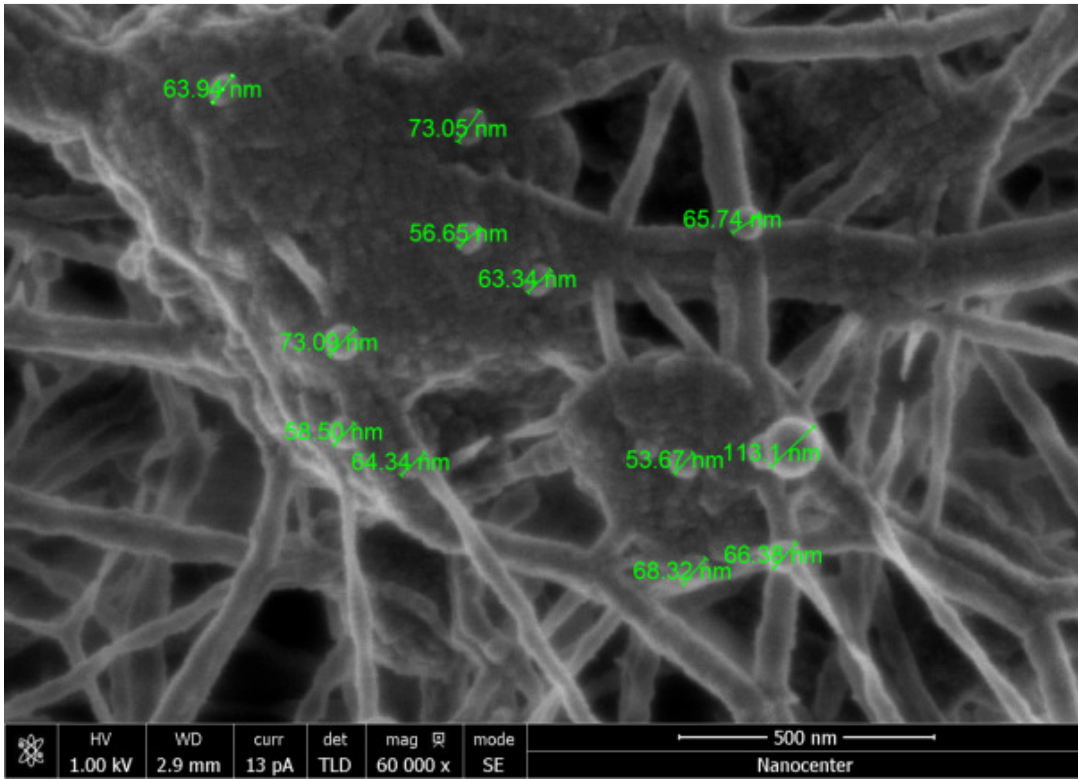
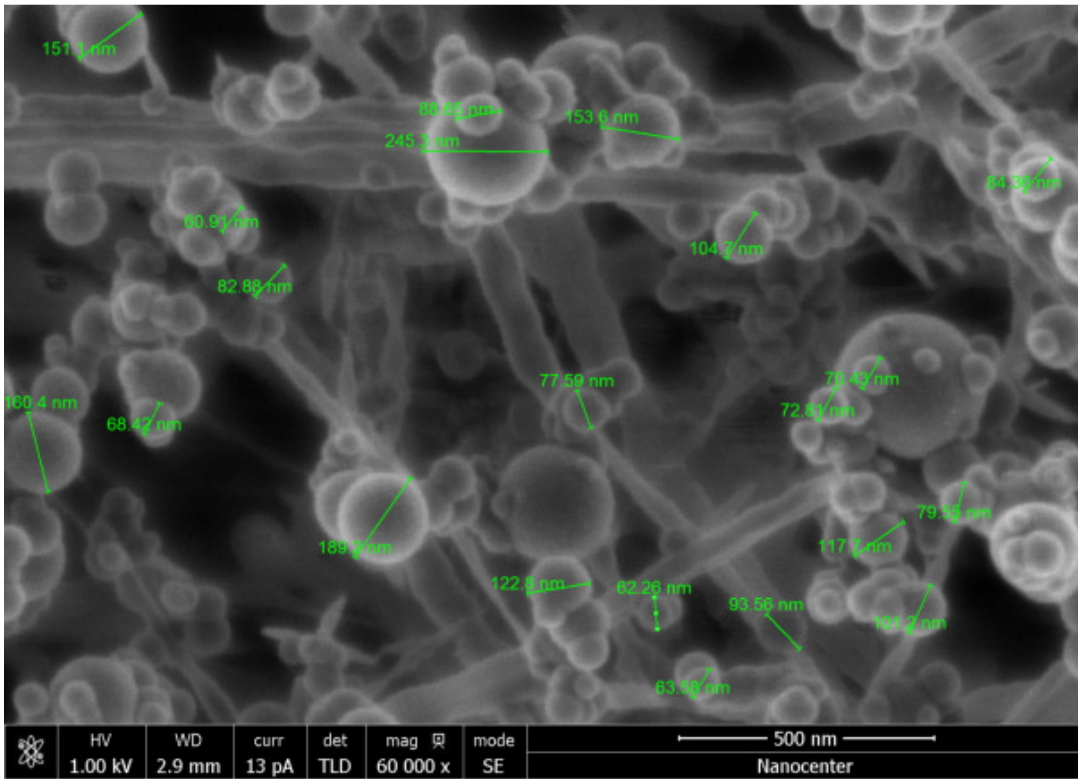


Figure S18. SEM image of N2 nigrosin particles (Image N2b\_004)



210 Figure S19. SEM image of N3 nigrosin particles (Image N3\_010)